

# Neutron-induced fission of even- and odd-mass plutonium isotopes within a four-dimensional Langevin framework

M. R. Pahlavani\* and S. M. Mirfathi†

*Department of Nuclear Physics, Faculty of Basic Science, University of Mazandaran, P.O. Box 47415-416, Babolsar, Iran*

(Received 12 May 2017; published 11 July 2017)

Neutron multiplicity prior to scission and evaluation of mass distribution of fission fragments with the fission time scale for neutron induced fission of plutonium isotopes are investigated using a dynamical Langevin approach. Also, mass yield of fragments and prompt neutron multiplicity in different time scales of the fission process are compared with experimental data. Reasonable agreement is achieved between calculated and available experimental data.

DOI: [10.1103/PhysRevC.96.014606](https://doi.org/10.1103/PhysRevC.96.014606)

## I. INTRODUCTION

Despite many experimental and theoretical studies about different kinds of fission, there is has not been a fully microscopic approach to study the kinematics as well as the dynamics of fission. Different semiclassical and semiempirical approaches have been developed to extensively investigate fission fragment mass distribution, prompt neutron multiplicity, fission cross sections, and other properties of fission statistics, which are important for both nuclear technologies and knowledge of nuclear energy [1–7].

Statistical frameworks, such as Weisskopf-type or Hauser-Feshbach, have ignored dynamical evolution of the fission process. On the other hand, experimental methods of fission [5,6] have been developed to measure the particle multiplicities from excited nuclei and have exceeded the values expected from statistical models. Therefore to reproduce fission characteristics accurately, it is essential to employ a dynamical treatment of the fissioning nucleus, which goes beyond the limitations of the statistical model, taking into account the dissipation effects of the fissioning system after formation of the compound nucleus and its evaluation until separation of fission fragments at the scission point based on the dynamical Langevin approach [8].

After successful application of Langevin equations in the neutron-induced fission of uranium isotopes and  $^{239}\text{Pu}$  at low-excitation energies [9,10], in the present study the neutron-induced fission of five plutonium isotopes ( $^{238}\text{Pu}$ ,  $^{239}\text{Pu}$ ,  $^{240}\text{Pu}$ ,  $^{241}\text{Pu}$ , and  $^{242}\text{Pu}$ ) are analyzed and compared with available experimental data. Time evaluation of fission fragment mass distribution, along with prompt neutron multiplicity and its sensitivity to the energy of the incident neutron, was studied to present more quantitative results.

Although most of plutonium isotopes, namely,  $^{238}\text{Pu}$ ,  $^{240}\text{Pu}$ , and  $^{242}\text{Pu}$ , are fissionable with fast neutrons and are significant in a fast neutron reactor, they are even- $A$  isotopes;  $^{241}\text{Pu}$  and  $^{239}\text{Pu}$  play a major role in the conventional light water power reactor and undergo fission with thermal neutrons. Therefore, the fissile plutonium isotopes and the active targets  $^{239}\text{Pu}$

and  $^{241}\text{Pu}$  are considered the most important isotopes with respect to the modeling of innovative cores required for fast generation-IV reactors [11,12]. Also  $^{238}\text{Pu}$ ,  $^{240}\text{Pu}$ , and  $^{242}\text{Pu}$ , which are produced in nuclear fuel through successive neutron captures and decay processes, are nonfissile and most of their available data are limited below the reaction threshold. In thermal systems, these nonfissile isotopes are typically produced faster than they are transmuted due to their long half-lives. To optimize design parameters and reduce operation margins in fast reactors, in which the harder neutron spectrum efficiently induces fission in these and other transuranic isotopes, it is important to have highly accurate nuclear data in the fast neutron region where these systems operate [13].

In the following we briefly describe the theoretical aspects of the present model. Then we compare evaluated results with the available experimental data. Finally we analyze the results of the present approach by comparing theoretical results and available experimental data.

## II. DESCRIPTION OF THE DYNAMICAL MODEL

The shape of a fissioning nucleus in the present study is restricted to the funny hills parametrization. The funny hills parameters  $c$ ,  $h$ , and  $\alpha$  represent the elongation, the neck thickness, and the asymmetry of the fissioning system, respectively. These variables define the shape of the fissioning compound system in cylindrical coordinates [14,15]:

$$\rho_s^2(z) = \begin{cases} (c^2 - z^2)(A_s + B_{\text{sh}} \frac{z^2}{c^2} + \alpha \frac{z}{c}) & \text{if } B_{\text{sh}} \geq 0, \\ (c^2 - z^2)(A_s + \alpha \frac{z}{c}) e^{(B_{\text{sh}} c z^2)} & \text{otherwise,} \end{cases} \quad (1)$$

where  $\rho_s$  and  $z$  are defined above as the radial coordinate of the compound nuclei and the coordinate along the symmetry axis, respectively. The quantity  $A_s$  is defined based on the conservation of nuclear volume as follows [15]:

$$A_s = \begin{cases} c^{-3} + B_{\text{sh}}/5 & \text{if } B_{\text{sh}} \geq 0, \\ -\frac{4}{3} \frac{B_{\text{sh}}}{\exp(B_{\text{sh}} c^3) + [1 + 1/(2 B_{\text{sh}} c^3)] \sqrt{-\pi B_{\text{sh}} c^3 \operatorname{erf}(\sqrt{-B_{\text{sh}} c^3})}} & \text{otherwise,} \end{cases} \quad (2)$$

while  $B_{\text{sh}} = 2h + (c - 1)/2$  stands for the nuclear shape function. Many recent studies have been performed on the

\*m.pahlavani@umz.ac.ir

†m.mirfathi@umz.ac.ir

basis of one-dimensional and multidimensional Langevin equations to analyze experimental data on the different features of fission reactions [16–19]. However, in the present study to measure the evolution of the funny hills shape, we have performed the extension of the three-dimensional Langevin dynamical model by adding the orientation degree of freedom (projection  $K$  of the total spin  $I$  to the symmetry axis of the nucleus) that describes the shape evolution of the fissioning nucleus [20–22]. Evolution of these coordinates is considered as the motion of Brownian particles which interact with a large number of internal degrees of freedom, constituting the surrounding “heat bath” in the present stochastic approach [23,24]. The coupled four-dimensional Langevin equations are used to calculate the evaluation of the funny hills shape coordinates as [23]

$$\frac{dq_i}{dt} = \frac{p_j}{m_{ij}}, \quad (3)$$

$$\begin{aligned} \frac{dp_i}{dt} = & -\frac{p_j p_k}{2} \frac{\partial}{\partial q_i} \left( \frac{1}{m_{jk}} \right) - \frac{\partial V}{\partial q_i} \\ & + T^2 \frac{\partial a}{\partial q_i} - \eta_{ij} \frac{dq_i}{dt} + g_{jk} \xi_j(t), \end{aligned} \quad (4)$$

where  $q_i = c, h$ , and  $\alpha$  are coordinates, and  $p_i = m_{ij} \frac{dq_j}{dt}$  are their conjugate momenta. Following the Maxwell-Boltzmann distribution the initial distribution of the coordinates and momenta for each Langevin trajectory are chosen from sampling random numbers [24–27]. The initial value of  $c$  is restricted to interval (1.00, 1.10). Also,  $V$  and  $a$  are, respectively, the potential energy of the system and the level density parameter, which are defined in the following.  $T$  is the temperature of the compound nucleus, which is related to its intrinsic energy through  $T = \sqrt{E_{\text{int}}/a}$ . The intrinsic energy of the compound system ( $E_{\text{int}}$ ) is recalculated at every step of the Langevin trajectory:

$$E_{\text{int}} = E_{\text{c.m.}} - Q - \frac{p_i p_j}{2 m_{ij}} - V(q, l, T = 0). \quad (5)$$

where  $E_{\text{c.m.}}$  and  $Q$  are the energy of the system in the center-of-mass framework and the  $Q$  value of the reaction, respectively.

The inertia tensor  $m_{ij}$  is evaluated using the Werner-Wheeler formula [28,29]:

$$m_{ij} = \pi \rho_m \int_{z_{\min}}^{z_{\max}} \rho_s^2(z) (A_i A_j + \rho_s^2(z) A_i' A_j' / 8) dz, \quad (6)$$

where  $\rho_m$ ,  $z_{\min}$ , and  $z_{\max}$  are the mass density of the compound nucleus and the left and the right boundaries of the compound nucleus surface, respectively.  $A_i$  can be expressed as

$$A_i = -\frac{1}{\rho_s^2(z)} \frac{\partial}{\partial q_i} \int_{-c}^z \rho_s^2(z') dz'. \quad (7)$$

The quantity  $A'$  is the first derivative of  $A$  with respect to  $z$ . The modified potential energy of the system consists of the liquid-drop, the rotational, and the microscopic parts [8,30]:

$$V(q, I, K, T) = V_{\text{LD}}(q) + V_r(q) + V_{\text{SH}}(q, T). \quad (8)$$

Here  $V_{\text{LD}}(q)$  is the potential energy, which is calculated based on the liquid-drop model as

$$V_{\text{LD}}(q) = E_S(q) + E_C(q), \quad (9)$$

where  $E_S$  and  $E_C$  are the surface and Coulomb energy, respectively [31]. The second term on the right-hand side of Eq. (5) is the so-called rotational energy:

$$\begin{aligned} V_r(q) = & \frac{[I(I+1) - K^2] \hbar^2}{I_{\perp}(q) 0.8 M R_0^2 + 8 M a_0^2} \\ & + \frac{K^2 \hbar^2}{I_{\parallel}(q) 0.8 M R_0^2 + 8 M a_0^2}, \end{aligned} \quad (10)$$

where  $R_0 = 1.2249 A_{\text{CN}}^{1/3}$ ,  $A_{\text{CN}}$  is the mass number of the compound nuclei (CN), and  $a_0 = 0.6$  fm [30]. The temperature-dependent shell correction energy as a microscopic part of the potential energy is denoted by  $V_{\text{SH}}$  as

$$V_{\text{SH}}(q, T) = [\Delta E_{\text{pair}}(q) + \Delta E_{\text{shell}}(q)] \Phi(T), \quad (11)$$

where  $\Delta E_{\text{pair}}(q)$  is the pairing correlation energy in the BCS approximation [14,32]. Also, based on the Strutinsky method the shell correction energy, which is denoted by  $\Delta E_{\text{shell}}(q)$ , is the difference between the sum of the single-particle energies of occupied states and the average density of single-particle states and can be evaluated using [14,33,34]

$$\Delta E_{\text{shell}}(q) = \sum_k \epsilon_k - \int_{-\infty}^{\mu} e g(e) de. \quad (12)$$

Here the energy, the chemical potential, and the parameter of density of states for the single-particle representation are, respectively, denoted by  $\epsilon_k$ ,  $\mu$ , and  $g(e)$ . The temperature dependence of the shell correction is [35]

$$\Phi(T) = \exp\left(-\frac{a T^2}{E_d}\right), \quad (13)$$

where  $E_d$  is the shell damping energy that is considered to be 25 MeV and  $a$  is the level density parameter, which is evaluated as follows [36,37]:

$$a = \left\{ 1 + \frac{V_{\text{SH}}(T=0)}{a T^2} \left[ 1 - \exp\left(-\frac{E_{\text{int}}}{E_d}\right) \right] \right\} \tilde{a}(q), \quad (14)$$

where in high-excitation energies the asymptotic form of  $a$  is defined by  $\tilde{a}$  as

$$\tilde{a}(q) = a_1 A_{\text{CN}} + a_2 A_{\text{CN}}^{2/3} B_s(q). \quad (15)$$

The average values of the volume and the surface coefficients of  $\tilde{a}(q)$ , which were used in the present study and control the volume and shape dependence of the level density parameter, are  $a_1 = 0.050$  and  $a_2 = 0.190$ , where  $a_1 = 0.068$  and  $a_2 = 0.213$  were frequently used in the earlier literatures

[36,37]. Also  $B_s(q)$  is the dimensionless functional of the surface energy in the liquid drop model (LDM) with a sharp surface [14].

The inertia and friction tensors may be related to the shell effects. Therefore, to account for these effects we need to consider the calculated microscopic transport coefficients, for example, within the linear response theory and the local harmonic approximation. Because the calculated friction tensor in this approach is much smaller than those calculated by the macroscopic model at low temperature, the macroscopic friction and inertia tensors are used in the present paper. It should be mentioned here that the role of shell effects in the collective inertia and the friction coefficients are complicated physical phenomenon and may require deep information about the structure of the compound system, which is out of the scope of this study. However, this would not affect much the final results of the present approach. The friction tensor in the wall-and-window one-body dissipation scheme for a small elongation before neck formation ( $c < c_{\text{win}}$ ) is given by [38]

$$\eta_{\text{wall}_{ij}}(c < c_{\text{win}}) = \frac{\pi \rho_m}{2} \bar{v} \int_{z_{\text{min}}}^{z_{\text{max}}} \left( \frac{\partial \rho_s^2}{\partial q_i} \right) \left( \frac{\partial \rho_s^2}{\partial q_j} \right) \times \left[ \rho_s^2 + \left( \frac{1}{2} \frac{\partial \rho_s^2}{\partial z} \right)^2 \right]^{-1/2} dz, \quad (16)$$

and for an elongation greater than those points in which a neck is formed in the nuclear system ( $c \geq c_{\text{win}}$ ), the corresponding friction tensors can be defined by [38]

$$\eta_{\text{wall}_{ij}}(c \geq c_{\text{win}}) = \frac{\pi \rho_m}{2} \bar{v} \left\{ \int_{z_{\text{min}}}^{z_{\text{neck}}} \left( \frac{\partial \rho_s^2}{\partial q_i} + \frac{\partial \rho_s^2}{\partial z} \frac{\partial D_1}{\partial q_i} \right) \times \left( \frac{\partial \rho_s^2}{\partial q_j} + \frac{\partial \rho_s^2}{\partial z} \frac{\partial D_1}{\partial q_j} \right) \times \left[ \rho_s^2 + \left( \frac{1}{2} \frac{\partial \rho_s^2}{\partial z} \right)^2 \right]^{-1/2} dz + \int_{z_{\text{neck}}}^{z_{\text{max}}} \left( \frac{\partial \rho_s^2}{\partial q_i} + \frac{\partial \rho_s^2}{\partial z} \frac{\partial D_2}{\partial q_i} \right) \times \left( \frac{\partial \rho_s^2}{\partial q_j} + \frac{\partial \rho_s^2}{\partial z} \frac{\partial D_2}{\partial q_j} \right) \times \left[ \rho_s^2 + \left( \frac{1}{2} \frac{\partial \rho_s^2}{\partial z} \right)^2 \right]^{-1/2} dz \right\}, \quad (17)$$

$$\eta_{\text{win}_{ij}}(c \geq c_{\text{win}}) = \frac{\pi \rho_m}{2} \bar{v} \left( \frac{\partial D_3}{\partial q_i} \frac{\partial D_3}{\partial q_j} \right) \Delta \sigma, \quad (18)$$

where  $\bar{v} = \frac{3}{4}v$  is the average speed of nucleons inside the nucleus with  $v$  is the Fermi velocity of the Fermi gas model.  $D_1$  and  $D_2$  represent the positions of the centers of two parts of a fissioning system, relative to the center of mass of the whole system.  $z_{\text{min}}$ ,  $z_{\text{max}}$ , and  $z_{\text{neck}}$  are the positions of the left and right ends of the nuclear shape and the neck plane, respectively. Also  $\Delta \sigma$  is the area of window between two parts

of the system and  $D_3$  is the distance between the centers of mass of the nascent fragments. Eventually, after introducing a measure of chaos for the classical linear response theory regarding one-body dissipation, a scaled version of the friction (the chaos-weighted wall-and-window friction) will be [39]

$$\begin{aligned} \eta_{ij}(c < c_{\text{win}}) &= \mu(c) \eta_{\text{wall}_{ij}}(c < c_{\text{win}}), \\ \eta_{ij}(c \geq c_{\text{win}}) &= \mu(c) \eta_{\text{wall}_{ij}}(c \geq c_{\text{win}}) + \eta_{\text{win}_{ij}}(c \geq c_{\text{win}}). \end{aligned} \quad (19)$$

Here  $\mu(c)$  is a random number that is a measure of chaos that is sampled following the Maxwell-Boltzmann distribution. To obtain variation of the shape of the compound nucleus from its initial spherical symmetric to deformed asymmetric shape,  $\mu(c)$  was sampled randomly in the range of 0 to 0.5.

The normalized random force  $g_{ij} \xi_j(t)$ , which is related to the dissipation coefficients through the fluctuation dissipation theorem, is assumed to be a Gaussian white noise and has an extremely short correlation time, implying that the intrinsic nuclear dynamics is Markovian. The strength of random force,  $g_{ij}$ , is given by  $\eta_{ij} T$  and the properties of  $\xi_j(t)$  can be written as [7,15,23,40]

$$\langle \xi_j(t) \rangle = 0, \quad \langle \xi_k(t_1) \xi_l(t_2) \rangle = 2\delta_{kl} \delta(t_1 - t_2), \quad (20)$$

which causes fluctuations of the collective variables resulting in fluctuations of the physical observables in the fission process. The  $\delta$  term means no time correlation among random forces and hence the collisions are memoryless. Moreover, the perturbation process of random force for each parameter does not mean that the value of the parameter is dependent on time. Actually, the realistic random force has little contribution to time through the collision time of particles. Also, application of Langevin equations is limited to the time scale greater than collision time, otherwise this approximation will not be valid.

The Langevin equation for the  $K$  coordinate allows the modeling of the relaxation process of  $K$  states depending on the instantaneous physical properties of the fissioning system, such as temperature and moment of inertia. The description of evolution of the  $K$  collective coordinate using the Langevin equation for overdamped motion has been recently proposed in Ref. [30]. The stochastic dynamics of the orientation degree of freedom could be described by the overdamped Langevin equation [15]:

$$dK = -\frac{I^2 \gamma_K^2}{2} \frac{\partial V}{\partial K} dt + \gamma_K I \xi(t) \sqrt{\frac{T}{2}}, \quad (21)$$

where  $I$  and  $K$  are the total spin and its projection on the symmetry axis, respectively.  $\gamma_K$  is the friction parameter, which controls the coupling between the orientation degree of freedom and the heat bath [15]:

$$\gamma_K = \frac{1}{R_N R_{\text{CN}} \sqrt{2\pi^3 n_0}} \sqrt{\frac{I_{\parallel} I_{\text{eff}} I_R}{I_{\perp}^3}}, \quad (22)$$

where  $R_N$  and  $n_0$  are the neck radius and the bulk flux in standard nuclear matter  $n_0 = 0.263 \times 10^{-22} \text{ MeV s fm}^{-4}$ .

$I_{\parallel}$  and  $I_{\perp}$  are the rigid-body moments of inertia about and perpendicular to the symmetry axis for a liquid-drop nucleus with a sharp boundary as a function of the distance between mass centers in units of the corresponding spherical values,

$$I_{\parallel} = c^2 \left\{ c^{-3} + \frac{4B_s}{35} \left( \frac{4B_s c^3}{15} - 1 \right) \right\}, \quad (23)$$

where  $I_{\perp} = I_{\parallel} + c^2$ . Also  $I_R = MR_{CN}^2/4$ , with  $M$  and  $R_{CN}$  being the mass and the radius of the compound nucleus, and  $I_{\text{eff}}^{-1} = I_{\parallel}^{-1} - I_{\perp}^{-1}$  is the effective moment of inertia. The initial value of  $K$  for each Langevin trajectory was generated from a uniform distribution as a function of angular momentum ( $L$ ), using the Monte Carlo method in the interval  $(-L, L)$  [30]. Also  $\xi(t)$  has the same meaning as in Eq. (4). The Langevin equations for the shape parameters [Eqs. (3) and (4)] and the Langevin equation for the  $K$  coordinate [Eq. (12)] are connected through the potential energy. The Langevin dynamics of the  $K$  coordinate is influenced by the actual value of the potential energy  $V(q, I, K, T)$ . At the same time, the rotational part of the potential energy is dependent on the actual  $K$  value at time  $t$ , and in this way it influences the dynamical evolution of the shape parameters.

In the present dynamical model, each fission event is defined as the instance when the Langevin trajectory overcomes the scission point and the neck radius becomes zero. Shape evolution of the compound nucleus proceeds in competition with particle and  $\gamma$ -ray emission with fission. In the present study the multiplicity of neutrons is calculated using Weisskopf's conventional evaporation theory under the following outline. The neutron decay width is calculated using the following relation [41,42]:

$$\Gamma_n = \frac{2m_n}{[\pi \hbar]^2 \rho_c(E_{\text{int}})} \int_0^{E_{\text{int}} - B_n} \rho_d(E_{\text{int}} - \varepsilon_n) \varepsilon_n \sigma_{\text{inv}} d\varepsilon_n, \quad (24)$$

where  $m_n$  is the reduced mass of the neutron with respect to the residual nucleus and  $B_n$  shows the binding energy of the compound nuclei. Also,  $\rho_c$  and  $\rho_d$  are the level densities of the compound and daughter nuclei, respectively.  $\varepsilon_n$  is the mean kinetic energy of the emitted neutrons and  $\sigma_{\text{inv}}(\varepsilon_n) = \pi R_n^2$  is the inverse cross section for the reaction  $(A-1) + n \rightarrow A$ . Also  $R_n$  can be evaluated via  $R_n = 1.21[(A-1)^{1/3} + 1] + 3.4/\sqrt{\varepsilon_n}$ .

Practically, distribution of a fragment's mass and fission cross section in the statistical model for neutron-induced fission reactions is obtained using a proper distribution function that depends on fission transmission coefficients. However, in the present dynamical approach, a Monte Carlo algorithm is applied to calculate the competition between neutron emission and fission [43]. The neutron decay width and the decay rates of fission, which depend upon the excitation energy, the spin, and the mass number of each nuclei, have been evaluated in every interval of time evolution of a fissioning nucleus by employing the Langevin equations.

To calculate the competition between neutron emission and fission by using the Monte Carlo technique, in the first step, a random number  $r$  on the half-open interval  $[0,1)$  is selected.

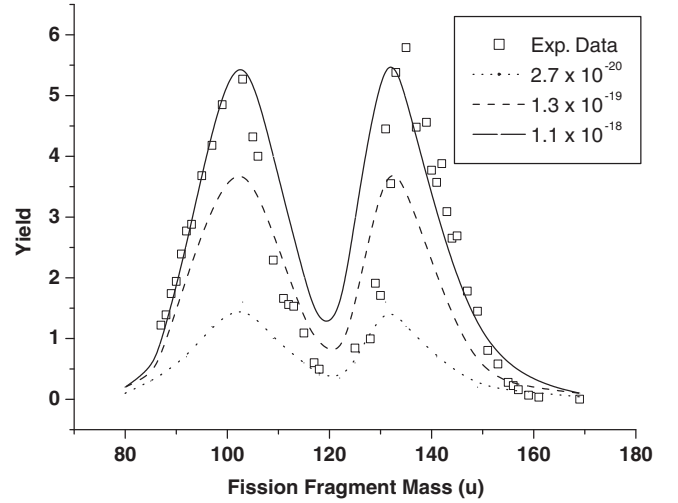


FIG. 1. Mass distribution of neutron-induced fission fragments of  $^{238}\text{Pu}$  with  $E_n = 0.0253$  eV. Experimental data [48] are indicated by open squares.

The random number is a numerical characteristic assigned to an element of the sample space. Then the probability of emission of a neutron is defined by  $x = \tau/\tau_n$ , where  $\tau_n$  is the neutron decay time and  $\tau$  is the time step of the calculation. If  $r < x$ , it will be interpreted as a neutron emission; otherwise if the neck radius is equal to zero, it will be clarified as fission, which determines the fission probability. After emission of a neutron, the intrinsic excitation energy of the residual nuclei is recalculated and the process is continued. The kinetic energy of the emitted neutrons has been sampled from the Watt spectrum [44,45]:

$$\frac{dN_{\text{pre}}}{d\varepsilon_n} = \frac{\sqrt{\varepsilon_n}}{\Gamma(3/2)\sqrt{T_{\text{pre}}^3}} \exp(-\varepsilon_n/T_{\text{pre}}). \quad (25)$$

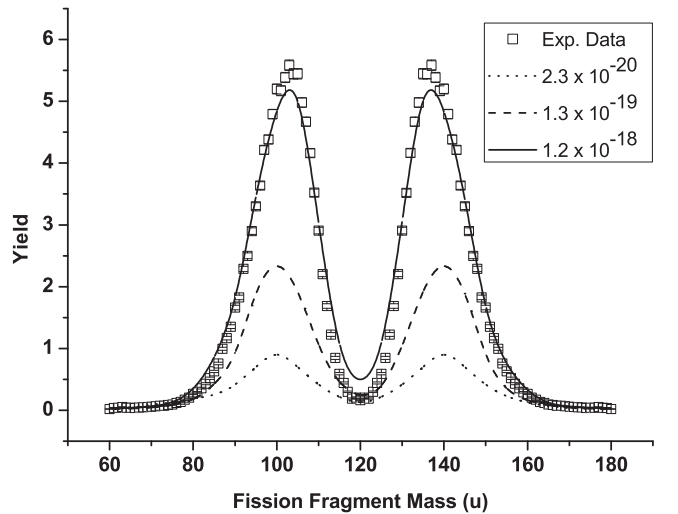


FIG. 2. Mass distribution of neutron-induced fission fragments of  $^{239}\text{Pu}$  with  $E_n = 0.0253$  eV. Experimental data [49] are indicated by open squares.

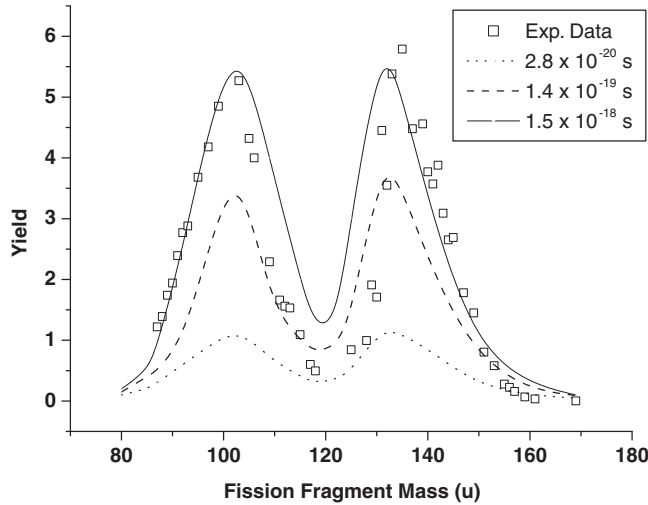


FIG. 3. Mass distribution of neutron-induced fission fragments of  $^{240}\text{Pu}$  with  $E_n = 1.9$  eV. Experimental data [50] are indicated by open squares.

Here we choose  $T_{\text{pre}} = 1.10 \pm 0.05$  MeV. After every fission event, the mass numbers of conjugate fragments are calculated as well. Calculation of the cross section for the neutron-induced fission reaction, based on an extended statistical model, predicts a significant change in the properties of fission fragments [46,47].

### III. RESULTS

We performed calculations for the compound nuclei formed in the following neutron-induced reactions:

- (I)  $n_{\text{th}} + {}^{238}\text{Pu}$  ( $E_n = 0.0253$  eV),
- (II)  $n_{\text{th}} + {}^{239}\text{Pu}$  ( $E_n = 0.0253$  eV),
- (III)  $n + {}^{240}\text{Pu}$  ( $E_n = 1.9$  eV),
- (IV)  $n_{\text{th}} + {}^{241}\text{Pu}$  ( $E_n = 0.0253$  eV),

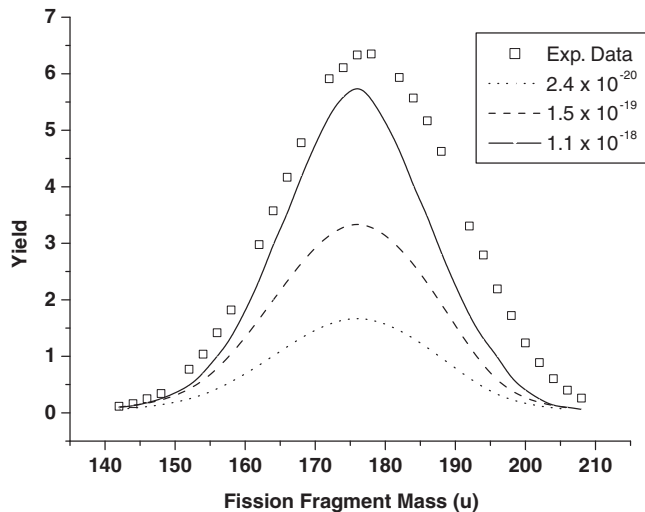


FIG. 4. Mass distribution of neutron-induced fission fragments of  $^{241}\text{Pu}$  with  $E_n = 0.0253$  eV. Experimental data [51] are indicated by open squares.

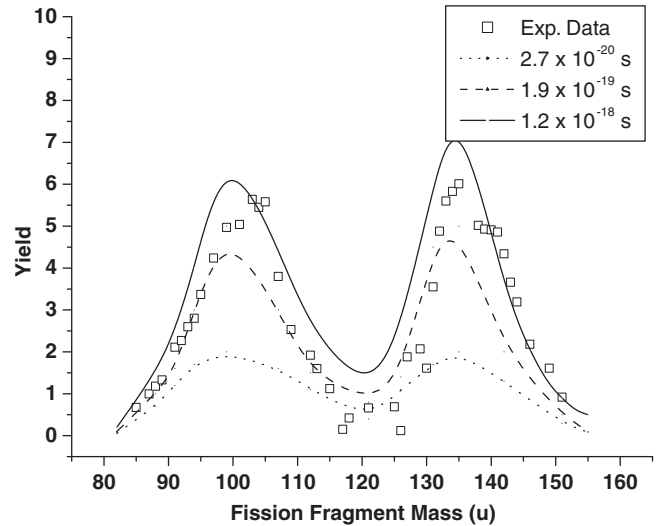


FIG. 5. Mass distribution of neutron-induced fission fragments of  $^{242}\text{Pu}$  with  $E_n = 15.1$  MeV. Experimental data [52] are indicated by open squares.

$$(V) \quad n + {}^{242}\text{Pu} (E_n = 15.1 \text{ MeV}).$$

The reason for selecting these reactions is that these reactions have been studied experimentally. Therefore a few experimental observables are available for comparison with the theoretical predictions.

To illustrate the variation of fission probability with time, the evaluation of the calculated mass distributions of fission fragments for the selected isotopes of plutonium together with experimental data are shown in Figures 1–5. In these figures the open squares indicate the experimental data [48–52] and the dashed, dotted, and solid lines represent the calculated results of the present dynamical approach for different times of fission.

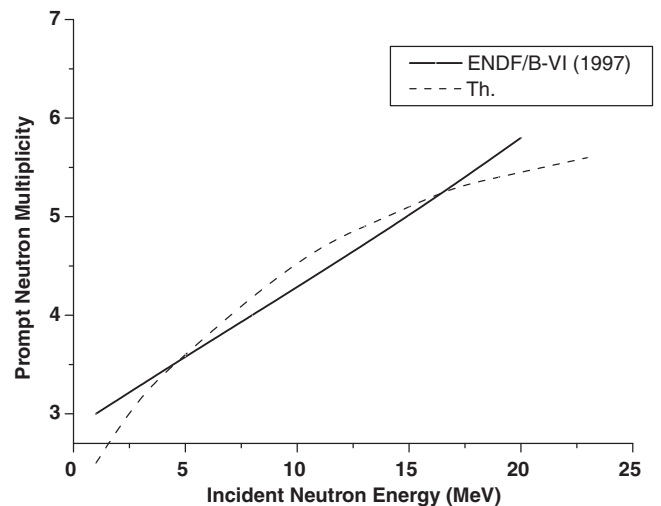


FIG. 6. Average prompt fission neutron multiplicity for  $^{238}\text{Pu}$  as a function of the incident neutron energy. Experimental data are denoted by the solid line.

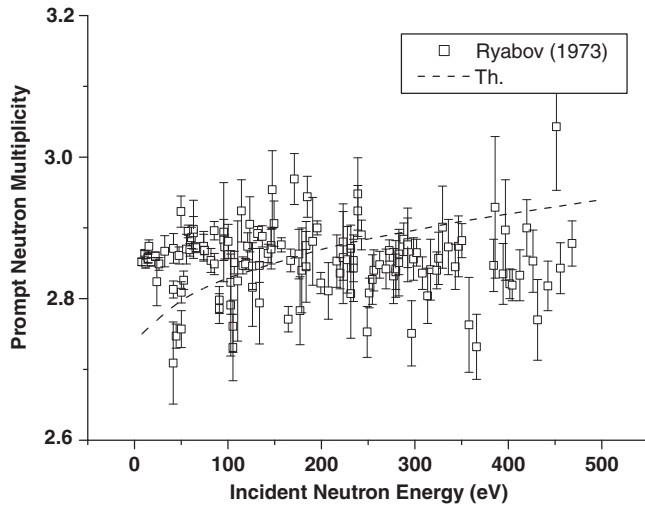


FIG. 7. Average prompt fission neutron multiplicity for  $^{239}\text{Pu}$  as a function of the incident neutron energy. Experimental data [53] are denoted by open squares.

The variation of these distributions with time are in accordance with general expectations. As can be seen in these figures the time it takes these nuclei bombarded with neutrons to descend from saddle to scission point is very long especially in the case of thermal neutrons for  $^{239}\text{Pu}$  and  $^{241}\text{Pu}$ . It is clear from these figures that the number of fission events increases with time until they become saturated, which indicates the occurrence of almost all of the fission events. As can be seen in these figures, the theoretical results and therefore the contributions of the mass-asymmetric fission events of plutonium isotopes have been clarified and are in agreement with available experiment data. Although as is clear from Figs. 1, 3, and 5, the theoretical mass yields of fission fragments for  $^{238}\text{Pu}$ ,  $^{240}\text{Pu}$ , and  $^{242}\text{Pu}$  obtained are a little bit higher than experimental data, and also the peak position of

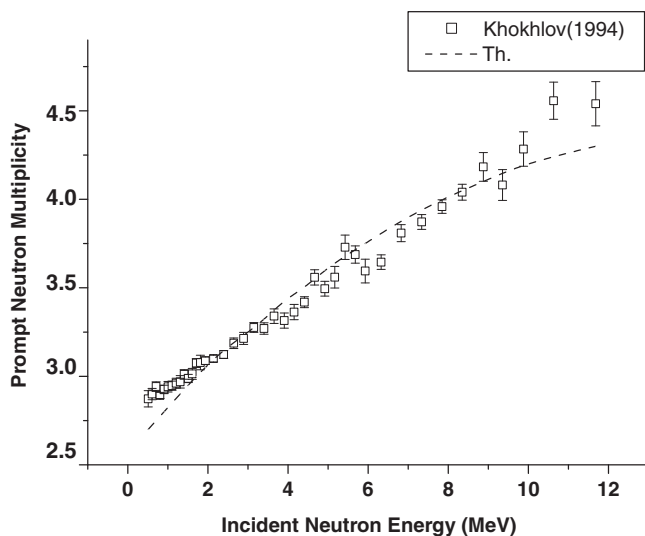


FIG. 8. Average prompt fission neutron multiplicity for  $^{240}\text{Pu}$  as a function of the incident neutron energy. Experimental data [54] are denoted by open squares.

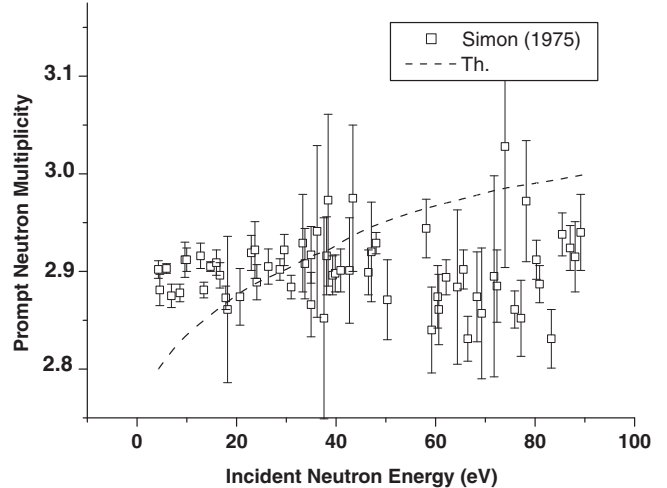


FIG. 9. Average prompt fission neutron multiplicity for  $^{241}\text{Pu}$  as a function of the incident neutron energy. Experimental data [55] are denoted by open squares.

the fragment yields is not in accordance with the experimental data but the widths of calculated mass distribution do not differ substantially from the experimental data. Also for  $^{239}\text{Pu}$  and  $^{241}\text{Pu}$  one can see in Figs. 2 and 4 that the theoretical mass yields of fragments obtained are a little bit lower than experimental data, but the peak position of the fragment yield is in accordance with the experimental data. Generally the presence and the position of each mass-asymmetric peak in these isotopes are reproduced rather well and the width and strength of the calculated mass distribution do not differ substantially from the experimental data.

The average neutron multiplicities as a function of incident neutron energy are also calculated and are shown in Figs. 6–10. These figures show a reasonable agreement of the theoretical result based on the dynamical approach with the experimental

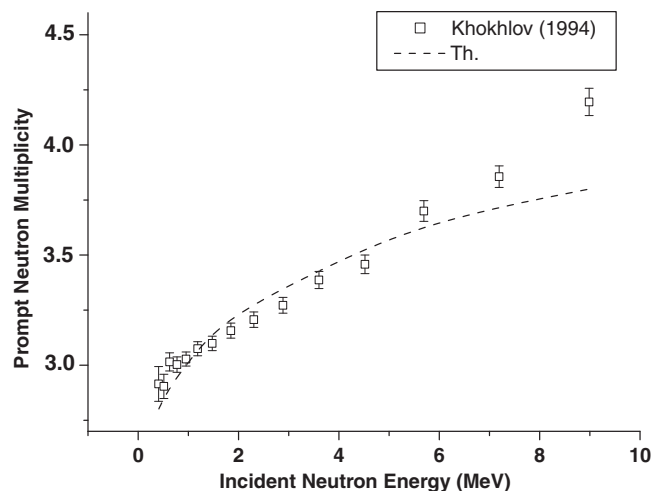


FIG. 10. Average prompt fission neutron multiplicity for  $^{242}\text{Pu}$  as a function of the incident neutron energy. Experimental data [54] are denoted by open squares.

data [53–55]. Although in low incident neutron energies, the agreement between results of the present model and the experimental data, which are denoted by solid squares, is satisfactory, but at high-excitation energies, such agreement is not achieved. Besides the incident energy of neutrons, the high average prompt neutron multiplicity is due to the effect of the fissility parameter, which plays an important role in theoretical calculation.

#### IV. CONCLUSION

In the present study, the neutron-induced fission of four plutonium isotopes was analyzed in terms of collective motion through the Langevin equations coupled with a Monte Carlo simulation to allow discrete emission of neutrons. The present dynamical Langevin mechanism was successful in calculating fission fragment mass distribution and in reproducing prompt

neutron multiplicity along with available experimental data. It was found that irrespective of the fissioning system the time evaluation of the mass yield of nascent mass fragments is insensitive to the energy of the incident neutron where we reproduce well the peak position of fragments for different isotopes. Generally with these theoretical considerations, the proportionality of emitted prompt neutrons versus incident neutron energies are consistent with the available experimental data. We obtained the sawtooth behavior of prompt neutron multiplicity that was observed experimentally. If we look at the trend of the theoretical multiplicity, a decrement is observed. This deviation in comparison with the experimental data is not so surprising since the prompt neutron multiplicity is mainly dependent on the total excitation energy of each nucleus, which is mainly related to incident neutron energies, and the parameters of the present model (such as friction coefficient), which are modified for low-energy-induced fission in the present model.

- 
- [1] H. Goutte, J. F. Berger, P. Casoli, and D. Gogny, *Phys. Rev. C* **71**, 024316 (2005).
- [2] S. Lemaire, P. Talou, T. Kawano, M. B. Chadwick, and D. G. Madland, *Phys. Rev. C* **73**, 014602 (2006).
- [3] J. Randrup and R. Vogt, *Phys. Rev. C* **80**, 024601 (2009).
- [4] P. Talou, B. Becker, T. Kawano, M. B. Chadwick, and Y. Danon, *Phys. Rev. C* **83**, 064612 (2011).
- [5] R. Vogt, J. Randrup, D. A. Brown, M. A. Descalle, and W. E. Ormand, *Phys. Rev. C* **85**, 024608 (2012).
- [6] B. Becker, P. Talou, T. Kawano, Y. Danon, and I. Stetcu, *Phys. Rev. C* **87**, 014617 (2013).
- [7] Y. Aritomo, S. Chiba, and F. Ivanyuk, *Phys. Rev. C* **90**, 054609 (2014).
- [8] Y. Aritomo and S. Chiba, *Phys. Rev. C* **88**, 044614 (2013).
- [9] M. R. Pahlavani and S. M. Mirfathi, *Phys. Rev. C* **93**, 044617 (2016).
- [10] M. R. Pahlavani and S. M. Mirfathi, *Eur. Phys. J. A* **52**, 95 (2016).
- [11] G. Rimpault, in *Proceedings of International Workshop on Nuclear Data Needs For Generation IV Nuclear Energy Systems, April 2005*, edited by P. Rullhusen (World Scientific, Singapore, 2006).
- [12] G. Rimpault, D. Bernard, D. Blanchet, C. Vaglio-Gaudard, S. Ravaux, and A. Santamaria, *Phys. Procedia* **31**, 3 (2012).
- [13] F. Tovesson, T. S. Hill, M. Mocko, J. D. Baker, and C. A. McGrath, *Phys. Rev. C* **79**, 014613 (2009).
- [14] M. Brack, J. Damgaard, A. S. Jensen, H. C. Pauli, V. M. Strutinsky, and C. Y. Wong, *Rev. Mod. Phys.* **44**, 320 (1972).
- [15] P. N. Nadtochy, E. G. Ryabov, A. E. Gegechkori, Yu. A. Anischenko, and G. D. Adeev, *Phys. Rev. C* **85**, 064619 (2012).
- [16] W. Ye, *Phys. Rev. C* **83**, 044611 (2011).
- [17] P. N. Nadtochy, A. Kelic, and K.-H. Schmidt, *Phys. Rev. C* **75**, 064614 (2007).
- [18] E. G. Ryabov, A. V. Karpov, P. N. Nadtochy, and G. D. Adeev, *Phys. Rev. C* **78**, 044614 (2008).
- [19] J. Sadhukhan and S. Pal, *Phys. Rev. C* **84**, 044610 (2011).
- [20] A. V. Karpov, P. N. Nadtochy, D. V. Vanin, and G. D. Adeev, *Phys. Rev. C* **63**, 054610 (2001).
- [21] P. N. Nadtochy, G. D. Adeev, and A. V. Karpov, *Phys. Rev. C* **65**, 064615 (2002).
- [22] G. D. Adeev, A. V. Karpov, P. N. Nadtochy, and D. V. Vanin, *Fiz. Elem. Chastits At. Yadra* **36**, 732 (2005).
- [23] Y. Abe, S. Ayik, P.-G. Reinhard, and E. Suraud, *Phys. Rep.* **275**, 49 (1996).
- [24] P. Frobrich and I. I. Gontchar, *Phys. Rep.* **292**, 131 (1998).
- [25] G. Chaudhuri and S. Pal, *Phys. Rev. C* **65**, 054612 (2002).
- [26] A. K. Dhara, K. Krishan, C. Bhattacharya, and S. Bhattacharya, *Phys. Rev. C* **57**, 2453 (1998).
- [27] G. Chaudhuri and S. Pal, *Phys. Rev. C* **63**, 064603 (2001).
- [28] H. Feldmeier, *Rep. Prog. Phys.* **50**, 915 (1987).
- [29] K. T. R. Davies, A. J. Sierk, and J. R. Nix, *Phys. Rev. C* **13**, 2385 (1976).
- [30] J. P. Lestone and S. G. McCalla, *Phys. Rev. C* **79**, 044611 (2009).
- [31] A. J. Sierk, *Phys. Rev. C* **33**, 2039 (1986).
- [32] S. G. Nilsson, C. F. Tsang, A. Sobczewski, Z. Szymański, S. Wycech, C. Gustafson, I. Lamm, P. Moller, and B. Nilsson, *Nucl. Phys. A* **131**, 1 (1969).
- [33] V. M. Strutinsky, *Nucl. Phys. A* **95**, 420 (1967).
- [34] F. A. Ivanyuk, S. Chiba, and Y. Aritomo, *Phys. Rev. C* **90**, 054607 (2014).
- [35] T. Asano, T. Wada, M. Ohta, T. Ichikawa, S. Yamaji, and H. Nakahara, *J. Nucl. Radiochem. Sci.* **5**, 1 (2004).
- [36] J. Toke and W. J. Swiatecki, *Nucl. Phys. A* **372**, 141 (1981).
- [37] A. V. Ignatyuk, M. G. Itkis, V. N. Okolovich, G. N. Smirenkin, and A. S. Tishin, *Yad. Fiz.* **21**, 1185 (1975).
- [38] D. V. Vanin, G. I. Kosenko, and G. D. Adeev, *Phys. Rev. C* **59**, 2114 (1999).
- [39] S. Pal and T. Mukhopadhyay, *Phys. Rev. C* **57**, 210 (1998).
- [40] Y. Aritomo and M. Ohta, *Nucl. Phys. A* **744**, 3 (2004).
- [41] V. Weisskopf, *Phys. Rev.* **52**, 295 (1937).
- [42] M. Blann, *Phys. Rev. C* **21**, 1770 (1980).
- [43] W. J. Swiatecki, K. Siwek-Wilczynska, and J. Wilczynski, *Phys. Rev. C* **78**, 054604 (2008).
- [44] Y. Jia and J. D. Bao, *Phys. Rev. C* **75**, 034601 (2007).

- [45] H. Rossner, D. J. Hinde, J. R. Leigh, J. P. Lestone, J. O. Newton, J. X. Wei, and S. Elfstrom, *Phys. Rev. C* **45**, 719 (1992).
- [46] H. Naik, V. K. Mulik, P. M. Prajapati, B. S. Shivasankar, S. V. Suryanarayana, K. C. Jagadeesan, S. V. Thakare, S. C. Sharmae, and A. Goswami, *Nucl. Phys. A* **913**, 185 (2013).
- [47] E. Birgersson, A. Oberstedt, S. Oberstedt, and F.-J. Hamsch, *Nucl. Phys. A* **817**, 1 (2009).
- [48] M. Haddad, J. Crançon, G. Lhospice, and M. Asghar, *Nucl. Phys. A* **481**, 333 (1988).
- [49] C. Tsuchiya, Y. Nakagome, H. Yamana, H. Moriyama, K. Nishio, I. Kanno, K. Shin, and I. Kimura, *J. Nucl. Sci. Tech.* **37**, 941 (2000).
- [50] D. R. Nethaway, A. L. Prindle, W. A. Myers, W. C. Fuqua, and M. V. Kantelo, *Phys. Rev. C* **16**, 1907 (1977).
- [51] N. P. D'yachenko, V. N. Kabenin, N. P. Kolosov, B. D. Kuz'minov, and A. I. Sergachev, *Prog. Yad.-Fiz. Issled. Rep.* **17**, 3 (1974).
- [52] I. Winkelmann and D. C. Aumann, *Phys. Rev. C* **30**, 934 (1984).
- [53] Yu. Ryabov, J. Trochon, D. Shackleton, and J. Frehaut, *Nucl. Phys. A* **216**, 395 (1973).
- [54] Yu. A. Khokhlov, I. A. Ivanin, V. I. In'kov, Yu. I. Vinogradov, L. D. Danilin, and B. N. Polynov, in *Proceedings of the International Conference on Nuclear Data for Science and Technology, 9–13 May, Gatlinburg, TN*, edited by J. K. Dickens (American Nuclear Society, 1994), Vol. 1, p. 272.
- [55] G. Simon and J. Frehaut, in *Proceedings of the Third All-Union Conference on Neutron Physics, Kiev, 9–13 June 1975* (International Atomic Energy Agency, Vienna, 1975), Vol. 5, p. 337.